Parallel inhomogeneous flows in a thermally anisotropic plasma: The electrostatic ion-acoustic branch

Robert S. Spangler and Earl E. Scime
Department of Physics, West Virginia University, Morgantown, West Virginia 26506

Gurudas I. Ganguli
Code 6794, Naval Research Laboratory, Washington, District of Columbia 20375

(Received 25 January 2002; accepted 1 April 2002)

The linearized dispersion relation describing waves in a plasma having a uniform magnetic field, uniform density, and inhomogeneous parallel (to the magnetic field) flow is generalized to include thermal anisotropy ($T_{i\perp}/T_{i\|}$), a key feature existing in many space and laboratory plasmas. The growth rate and the real frequency at which the maximum growth rate occurs for the ion acoustic mode increases with increasing $T_{i\perp}/T_{i\|}$. The propagation angle, with respect to the background magnetic field, for ion acoustic waves is shown to depend on $T_{i\perp}/T_{i\|}$. Also presented is a generalized calculation of experimentally relevant perturbed distribution functions to include shear in the field-aligned flow. © *2002 American Institute of Physics.* [DOI: 10.1063/1.1480269]

I. INTRODUCTION

High-resolution observations of ionospheric and magnetospheric phenomena are now routinely obtained by modern space probes, such as Viking, Freja, FAST (Fast Auroral SnapshoT), AMICIST (Auroral Microphysics and Ion Conics: Investigation of Space and Time), and Auroral Turbulence-2. A major revelation from these missions has been that the auroral region is highly structured with spatial scale sizes as small as a few ion gyroradii. Localized static (or quasi-static) electric fields both perpendicular[1–3] and parallel[4] to the magnetic field were found to be co-located with waves and coherent structures as well as with enhanced ion temperatures.[5–9] While recent theoretical and experimental work has demonstrated that perpendicular, localized electric fields can account for many of the phenomena observed in the auroral region,[10,11] some observations, e.g., localized field-aligned flows correlated with ion-acoustic-like features in wave spectra, remain unexplained.

By using the kinetic model developed by Ganguli *et al.*,[12] Gavrishachaka *et al.* demonstrated that a perpendicular gradient in the parallel flow (parallel flow shear) can lower the threshold current for the ion-acoustic mode below that of the ion-cyclotron mode and allows it to propagate even when the ion temperature (T_i) exceeds the electron temperature (T_e).[13,14] Typically, ion Landau damping prevents ion acoustic instabilities from growing in a plasma with comparable ion and electron temperatures. The simplified ion acoustic mode dispersion relation modified by parallel flow shear is given by[13]

$$\omega = k_z C_s \sigma + i(\text{Landau Resonance Terms}), \tag{1}$$

where

$$\sigma^2 = 1 - \frac{k_y}{k_z}\frac{dV_d}{dx}\frac{1}{\Omega_i}. \tag{2}$$

Here $V_d(x)$ is the inhomogeneous flow along the magnetic field (B_0) in the z direction, k_y and k_z are wave numbers in the y and z directions, $\omega = \omega_r + i\gamma$ is the complex wave frequency, and $C_s = (T_e/m_i)^{1/2}$ is the sound speed. For no shear ($dV_d/dx = 0$), the classical ion-acoustic limit is recovered. If $\sigma^2 < 0$, then the standard nonresonant D'Angelo instability around $\omega_r = 0$ in the drifting ion frame is recovered.[15] The $\sigma^2 > 0$ regime (except for the uniform $\sigma^2 = 1$ case) was recently addressed by Gavrishachaka *et al.*[13] For $\sigma^2 > 1$, shear increases the parallel phase speed (ω_r/k_z) of the ion acoustic mode by a factor of σ [see Eq. (1)] and leads to a broadband frequency spectrum in the sub-cyclotron range. For sufficiently large σ, the phase speed increases so much that ion Landau damping is greatly reduced. This leads to a much lower threshold current for the current-driven ion acoustic mode and it can grow even for $T_i \geqslant T_e$.[13] For wave propagation nearly perpendicular to B_0 ($k_y/k_z \gg 1$), the magnitude of shear, i.e., dV_d/dx, needed to reduce the instability threshold is very small. Gavrishachaka *et al.* suggested that such instabilities could explain the frequent observation of ion-acoustic like waves in ionospheric plasma where $T_i \sim T_e$.[9,16–18]

Measurements consistent with the observation of parallel shear modified ion-acoustic instabilities have been reported in the literature. The University of Iowa Q-Machine group reported observations of ion-acoustic-like waves in a $T_i = T_e$ alkali metal plasma only when the parallel flow shear was such that $\sigma^2 > 1$.[19] The Q-Machine group at West Virginia University has also reported similar observations of ion-acoustic-like waves in the presence of parallel flow shear.[20] Both experimental results are consistent with the theoretical predictions and demonstrate that parallel flow shear can significantly lower the threshold current for ion-acoustic instabilities. While Gavrishchaka's calculations include important spatial inhomogeneities, and therefore, account for small-scale structures in the ionosphere,[21] they do not include temperature anisotropy. Temperature anisotropy can significantly alter the dispersive properties of the plasma medium.[22] For example, increased ion temperature anisot-

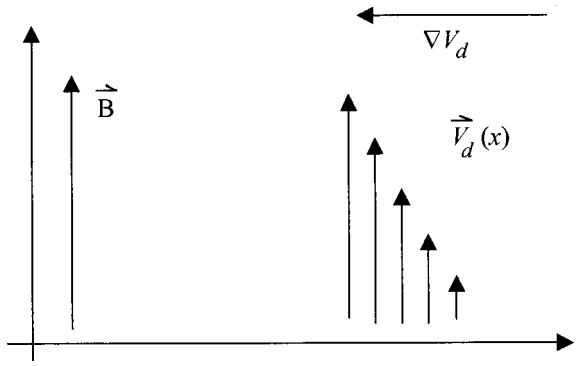

FIG. 1. Geometry of flow shear. For $\rho_i \ll L$, $\chi_g \approx x$.

ropy has been shown to increase the real frequency and growth rate of the electromagnetic Alfvén ion cyclotron instability.[23] Ion temperature anisotropy is routinely observed in Q-machine experiments,[20] in space,[5,24] and in other laboratory experiments designed to investigate space plasma phenomena.[25] In this work, we extend the theory to include temperature anisotropy and parallel flow shear.

In Sec. II, the general principles of the calculation are discussed. Some of the details and discussions of the validity of the calculations are placed in the Appendices. Numerical solutions of the dispersion relationship are reviewed in Sec. III and the results discussed in terms of space and laboratory measurements in Sec. VI.

II. THEORY

A kinetic model for electrostatic instabilities in a plasma having a uniform magnetic field along the z direction and inhomogeneous field-aligned flow was developed by Ganguli *et al.*[12] and used to investigate both ion acoustic and ion cyclotron modes by Gavrishachaka *et al.*[13,14] To study the effects of thermal anisotropy, we have generalized the formalism to include temperature anisotropy and have distinguished between parallel and perpendicular ion and electron temperatures throughout the analysis. The geometry of the parallel flow shear is described in Fig. 1. A first-order perturbed distribution function is developed by using the linearized Vlasov equation. Integration over all velocities yields a perturbed density. Separate perturbed densities for the ions and electrons are then substituted into Poisson's equation. The result is a self-consistent dispersion relation for plasma instabilities. To describe the plasma environment presented in Fig. 1, a zeroth-order distribution function describing inhomogeneous flow is used

$$f_0(H_\perp, H_\parallel, \chi_g) = C e^{-2\beta_\parallel H_\parallel(\chi_g)} e^{-2\beta_\perp H_\perp}, \tag{3}$$

where $H_\parallel(\chi_g) \equiv (v_\parallel - V_d(\chi_g))^2/2$, $H_\perp \equiv v_\perp^2/2$, $\beta_\parallel \equiv \frac{1}{2} v_{\mathrm{th}\parallel}^2$, $\beta_\perp \equiv \frac{1}{2} v_{\mathrm{th}\perp}^2$, $C \equiv n_0 \beta_\parallel^{1/2} \beta_\perp / \pi^{3/2}$, V_d is the parallel (field-aligned) flow, $v_{\mathrm{th}\perp}$ is the thermal velocity in the perpendicular direction, $v_{\mathrm{th}\parallel}$ is the thermal velocity in the parallel direction, n_o is the spatially uniform plasma density, and $\chi_g = x + v_y/\Omega$ is the guiding center position. The weak shear limit, $\rho_i \ll L = V_d/(dV_d/dx)$, is assumed so that $\chi_g \approx x$. Transforming all flows into the ion frame, keeping only the lowest order ($n = 0$) term for electrons (because $\omega \ll \Omega_{ce}$), and assuming the magnitude of the parallel flow shears are the same for electrons and ions, the dispersion relationship for electrostatic waves in a homogeneous plasma with sheared parallel flow and thermal anisotropy reduces to[26]

$$k^2 \lambda_{Di\perp}^2 + \frac{T_{\perp i}}{T_{\parallel i}} + \sum_{n=-\infty}^{\infty} \Gamma_n(b) F_{ni} + \tau \frac{T_{\perp e}}{T_{\parallel e}} (1 + F_{0e}) = 0, \tag{4}$$

where

$$F_{n,i} = \left(\frac{1}{\sqrt{2} k_\parallel v_{\mathrm{th}\parallel i}} \right) \left(n\Omega \left(1 - \frac{T_{\perp i}}{T_{\parallel i}} \right) + \frac{T_{\perp i}}{T_{\parallel i}} \omega \right) Z\left(\frac{\omega - n\Omega}{\sqrt{2} k_\parallel v_{\mathrm{th}\parallel i}} \right) - \frac{T_{\perp i} V_o'(x)}{T_{\parallel i} \Omega u} \left(1 + \left(\frac{\omega - n\Omega}{\sqrt{2} k_\parallel v_{\mathrm{th}\parallel i}} \right) Z\left(\frac{\omega - n\Omega}{\sqrt{2} k_\parallel v_{\mathrm{th}\parallel i}} \right) \right)$$

and

$$F_{0e} = \left(\frac{1}{\sqrt{2} k_\parallel v_{\mathrm{th}\parallel e}} \right) (\omega - k_\parallel V_d(x)) Z\left(\frac{\omega - k_\parallel V_d(x)}{\sqrt{2} k_\parallel v_{\mathrm{th}\parallel e}} \right) + \frac{V_d'(x)}{u \mu \Omega} \left(1 + \left(\frac{\omega - k_\parallel V_d(x)}{\sqrt{2} k_\parallel v_{\mathrm{th}\parallel e}} \right) Z\left(\frac{\omega - k_\parallel V_d(x)}{\sqrt{2} k_\parallel v_{\mathrm{th}\parallel e}} \right) \right).$$

$\mu \equiv M_i/M_e$, $u \equiv k_z/k_y$, $k_z = k_\parallel$, $b \equiv k_\perp^2/2\Omega^2 \beta_\perp$, $\Gamma_n \equiv e^{-b} I_n(b)$, $\tau \equiv T_{\perp i}/T_{\perp e}$, and $\lambda_{\mathrm{Di}\perp}^2 = M v_{\mathrm{th}\perp i}^2/4\pi e^2 n_0$ is the ion "perpendicular" Debye length. The first term in Eq. (4) describes the Debye shielding effects, the next two terms describe the ion response to the wave, and the last two terms describe the electron response. In the isotropic limit, the dispersion relation of Gavrishchaka *et al.* is recovered.[13] With the flow gradient set to zero, the dispersion relation for a thermally anisotropic plasma with current is recovered.[22] The only new term appearing in the ion response due to the inclusion of ion temperature anisotropy, the $n\Omega$ term, suggests that the effect of adding anisotropy can significantly alter the higher harmonic terms ($n > 0$) in the ion response to the wave fields. For example, for waves with frequencies near the ion cyclotron frequency, $\omega \sim \Omega$, and modest ion temperature anisotropy, $T_{i\perp}/T_{i\parallel} > 1$, both the sign and magnitude of the first term in the ion response change because of the new anisotropy term. The anisotropy effect is in addition to the parallel velocity shear term and thus, as will be shown later, affects the dispersion relationship in the case of small or zero shear. Another important feature of Eq. (4) is that the perpendicular ion temperature multiplies every term except the $n\Omega$ term.

A key step in the derivation of the dispersion relation is the integration of the perturbed distribution functions due to electrostatic waves in a thermally anisotropic medium. Perturbed distribution functions as a function of individual velocity components can be directly compared to plasma observations by measuring the component of the Doppler shifted absorption profile of metastable ions that oscillate at the wave frequency.[27–29] Because of their potential for experimental identification of specific instabilities, the perturbed distribution functions derived for these calculations are reproduced here

$$f_{1k}(v_\parallel) = -\frac{2qn_o\varphi_{1k}}{M\sqrt{\pi}}\sqrt{\beta_\parallel}\beta_\perp e^{-2\beta_\parallel(v_\parallel - V_d(x))^2}\left[1 - \sum_{m=-\infty}^{\infty}\Gamma_m(b)\left(\frac{(\omega - k_\parallel v_\parallel) + T_\perp/T_\parallel(v_\parallel - V_d(\chi_g))(k_\parallel - V_d'(\chi_g)k_y/\Omega)}{\omega - m\Omega - k_\parallel v_\parallel}\right)\right], \tag{5}$$

$$f_{1k}(v_y) = \frac{-qn_o\varphi_{1k}}{M}\frac{1}{v_{\text{th}\parallel}^2}f_o(v_y)e^{c^2/4_e\, a^2/8_e\, i/\Omega(v_y k_x)}\sum_{m,n=-\infty}^{\infty}\left(\frac{T_\parallel}{T_\perp}(\xi_0 - \xi_{m+n})Z(\xi_{m+n}) + (1 + \xi_{m+n}Z(\xi_{m+n}))\left(1\frac{k_y V_d'}{k_\parallel\Omega}\right)\right)e^{i(m+n)\theta}e^{-im\pi/2}J_m\left(\frac{v_y k_\perp}{\Omega}\right)\sum_{j=-\infty}^{\infty}e^{-ij\pi/2}I_j\left(\frac{ac}{2}\right)I_{n-j/2}\left(\frac{a^2}{8}\right), \tag{6}$$

where $a^2 \equiv k_\perp^2/\Omega^2\beta_\perp$ and $c^2 \equiv k_y^2/\Omega^2\beta_\perp$. Apart from a factor of $1/\pi$ in the amplitude, in the zero-shear limit Eq. (6) reduces to the same expression obtained by previous groups.[28]

The first order perturbed distribution function is a one-dimensional (in velocity space) description of the velocity dependent interaction of each particle with the wave fields for times prior to the moment of measurement. Experiments performed in laboratory plasmas have demonstrated that electrostatic wave amplitudes and wavelengths (assuming a particular dispersion relationship to eliminate either $k_\perp$ or $k_\parallel$) can be noninvasively measured by comparing laser induced fluorescence (LIF)[30] measurements of the perturbed distribution function to theoretical expressions.[27–29] For those experiments, the data were compared to theoretical expressions that included the effects of thermal anisotropy and parallel flow, but not shear in the parallel flow. However, this work has focused on the development of a more general theory for use in experiments with both parallel flow shear and thermal anisotropy. In the zero shear limit, $f_1(v_\parallel)$ depends only on $k_\perp$. Without the shear in the parallel flow to break the cylindrical symmetry, there is nothing unique about any direction perpendicular to the field and the perpendicular wave vector information vanishes during the angular integration.[31] With shear in the parallel flow, a unique shear direction is defined and two components of the wave vector ($k_\parallel$ and k_y) appear in $f_1(v_\parallel)$. In the local limit, the shear is defined to be along one axis (the x axis), but not the other (the y axis). One effect of velocity shear may be to provide a means of determining both $k_\parallel$ and k_y from measurements of $f_1(v_\parallel)$. The normalized shear term in Eq. (5) is multiplied by the quantity $k_y/k_\parallel$. If the wave amplitude and shear are directly measured (perhaps with a single probe and a parallel LIF measurement), comparison of an experimentally measured $f_1(v_\parallel)$ with numerically generated curves could be used to simultaneously determine $k_\parallel$ and $k_y/k_\parallel$. Note that such measurements would only yield the $k_\parallel$ and k_y for the most strongly growing mode.

III. ION ACOUSTIC INSTABILITIES

The generalized dispersion relation was investigated by numerically solving a dimensionless version of Eq. (4) (see Appendix A). Because the dispersion relation can be expressed solely as a function of $k_y\rho_i$, $k_\parallel/k_y$, $T_{i\perp}/T_{i\parallel}$, $T_{e\perp}/T_{e\parallel}$, $T_{i\perp}/T_{e\perp}$, and $V_d/v_{i\text{th}\perp}$, the numerical results only depend on the absolute temperature of either species through the gyroradius term in $k_y\rho_i$ and the normalized relative drift velocity, $V_d/v_{i\text{th}\perp}$. For a solution to the dispersion relation at a particular value of $k_y\rho_i$ and $V_d/v_{i\text{th}\perp}$, only the magnitudes of the actual perpendicular wave number and relative drift speed depend on the choice of perpendicular ion temperature, i.e., the form of the solution remains unchanged and the effects of temperature components (e.g., $T_{i\perp}$) need not be considered individually.

The classical current-driven ion acoustic instability[32] occurs at small values of $k_y\rho_i$ ($k_y\rho_i \ll 1$). Ion-acoustic (small $k_y\rho_i$) mode growth rates, γ, as a function of real frequency for varying values of ion temperature anisotropy are shown in Fig. 2. The mode described by Fig. 2 is identified as the ion-acoustic mode since it has a small (but nonzero) real frequency in an isotropic plasma with magnitude approximately equal to $k_\parallel C_s$. The growth rate results for the isotropic case shown in Fig. 2 are identical to previous calculations.[14] The plasma parameters used in the calculations for Fig. 2 are $T_{i\perp}/T_{e\perp} = 0.3$, $M_i/M_e = 29\,392$ (O^+ plasma), $V_d/v_{i\text{th}\perp} = 60$, and $|V_d'|/\Omega = 0.5$. Oxygen ions were used to facilitate comparison with the Gavrishchaka *et al.* calculations for oxygen ions in ionospheric plasmas. The growth rate curves were generated by fixing $b = (k_y\rho_i)^2$ at the same value used by Gavrishchaka *et al.*,[13] $(k_y\rho_i)^2 = 0.0675$, and varying u, where $u = k_z/k_y$, until the peak growth rate was obtained for each value of real frequency. For the isotropic case, u is varied such that $0.004 \leqslant u \leqslant 0.64$. Maximization over both wave vector parameters is usually required to find the peak growth rate. However, in

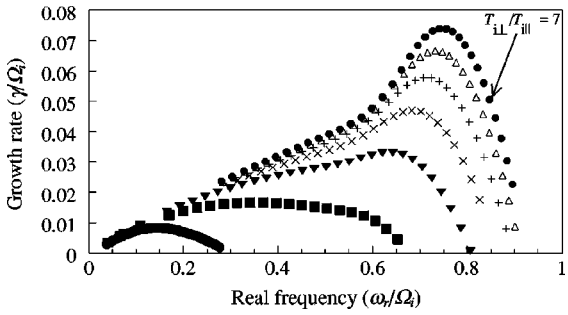

FIG. 2. Growth rate versus real frequency for the ion acoustic mode in plasmas with ion temperature anisotropies of (●) $T_{i\perp}/T_{i\parallel} = 1$, (■) $T_{i\perp}/T_{i\parallel} = 2$, (▼) $T_{i\perp}/T_{i\parallel} = 3$, (×) $T_{i\perp}/T_{i\parallel} = 4$, (+) $T_{i\perp}/T_{i\parallel} = 5$, (△) $T_{i\perp}/T_{i\parallel} = 6$, and (●) $T_{i\perp}/T_{i\parallel} = 7$. For these calculations, $T_{i\perp}/T_{e\perp} = 0.3$, $M_i/M_e = 29\,392$, $V_d/v_{i\text{th}\perp} = 60$, and $|V_d|/\Omega = 0.5$.

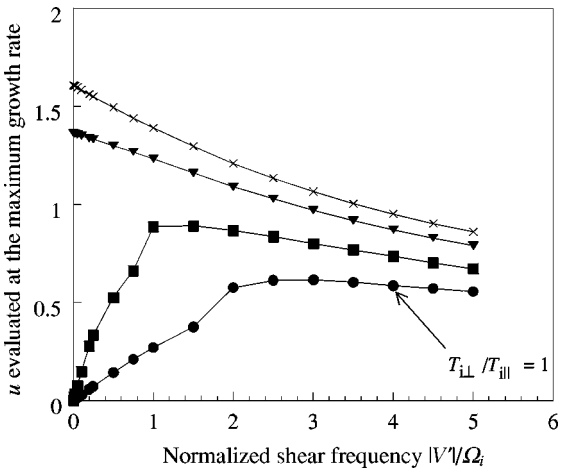

FIG. 3. u versus normalized shear for (●) $T_{i\perp}/T_{i\|}=1$, (■) $T_{i\perp}/T_{i\|}=2$, (▼) $T_{i\perp}/T_{i\|}=4$, and (×) $T_{i\perp}/T_{i\|}=6$. u is evaluated at the maximum growth rate for each case. For these calculations, $T_{i\perp}/T_{e\perp}=0.3$, $M_i/M_e=29\,392$, and $V_d/v_{i\mathrm{th}\perp}=60$.

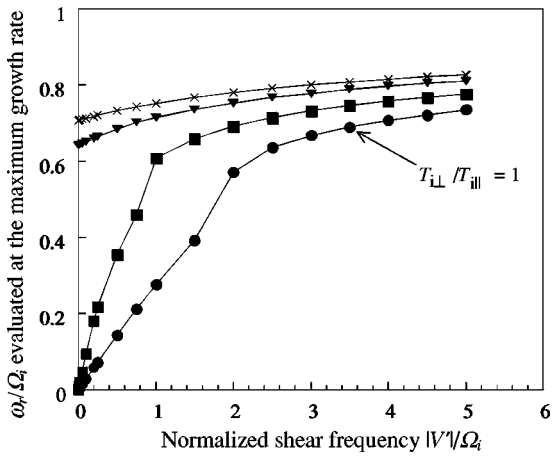

FIG. 4. Real frequency versus normalized shear for (●) $T_{i\perp}/T_{i\|}=1$, (■) $T_{i\perp}/T_{i\|}=2$, (▼) $T_{i\perp}/T_{i\|}=4$, and (×) $T_{i\perp}/T_{i\|}=6$. The real frequencies are for the modes with the largest growth rates at each shear value. For these calculations, $T_{i\perp}/T_{e\perp}=0.3$, $M_i/M_e=29\,392$, and $V_d/v_{i\mathrm{th}\perp}=60$.

this analysis b was fixed to the same value for all ion acoustic graphs because the growth rate was found to have a weak dependence on $k_y\rho_i$. Depending on the anisotropy, the effect of varying $k_y\rho_i$ is either negligible or slightly increases the frequency upshift of the growth rate curves (see Appendix B).

The real frequency of the ion-acoustic mode is found to strongly depend on the ion temperature anisotropy. The real frequency at the maximum growth rate corresponding to $T_{i\perp}/T_{i\|}=1$ is consistent with previous calculations[13] and the growth rate increases with increasing thermal anisotropy (Fig. 2). The approximate (keeping only $n=0$ terms) dispersion relation for ion acoustic waves in an anisotropic plasma

$$\omega \approx (k_\|)\sqrt{\frac{T_{\|e}}{M}\left(1-\frac{V_d'(x)}{\Omega u}\right)}, \tag{7}$$

does not explicitly depend on ion temperature anisotropy. Equation (7) is equivalent to the simplified expression derived by Gavrishchaka *et al.*,[13] except that the relevant electron temperature is the parallel electron temperature. Clearly, there is no explicit ion temperature anisotropy dependence in Eq. (7). Rewriting Eq. (7) in terms of the dimensionless ratios used in Appendix A yields

$$\hat{\omega} \approx u(k_y\rho)\sqrt{\left(\frac{1}{\tau\hat{T}_e}\right)\left(1-\frac{V_d'(x)}{\Omega u}\right)}, \tag{8}$$

where $\hat{\omega}\equiv\omega/\Omega$, $\hat{T}_e\equiv T_{e\perp}/T_{e\|}$, $\tau\equiv T_{i\perp}/T_{e\perp}$. Since $\hat{T}_e$, τ, $k_y\rho_i$, and V_d' are all held constant for the numerical calculations shown in Fig. 2, the dependence of the real frequency on the ion temperature anisotropy must be due to a dependence of the wave vector ratio, u, at growth peak rate on ion temperature anisotropy. The dependence of u at peak growth rate on the ion temperature anisotropy can be seen in Fig. 3 by comparing the values of u for different values of ion temperature anisotropy for a fixed value of shear. The wave vector ratio of $u=0.14$ for maximum growth rate at a shear of $|V_d'|/\Omega=0.5$ in an isotropic plasma is the same value as reported previously.[13]

Ion acoustic waves in plasmas without shear or thermal anisotropy propagate along the magnetic field, corresponding to a large value for u. In the presence of an inhomogeneous parallel flow, an ion acoustic wave in an isotropic plasma propagates obliquely.[13] Figure 3 indicates that as $T_{i\perp}/T_{i\|}$ increases, the ion acoustic wave propagation becomes more parallel to the magnetic field. The change in u, however, is less dramatic as the shear increases. At large values of normalized shear, the trend is for u's of all anisotropy values to approach each other. As the magnitude of the shear is increased, the effects of anisotropy become less apparent for the propagation angle and the real frequency, but the effect of anisotropy on the growth rate appears unaffected. As a check of the approximate dispersion relationship, the real frequencies predicted by Eq. (8) were determined for the values of u extracted from Fig. 3 and compared to the numerical solutions to Eq. (4). The real frequencies from both methods were nearly identical. Figure 2 also shows that the frequency spectrum initially becomes broader as $T_{i\perp}/T_{i\|}$ is increased from the isotropic case. At larger values of ion temperature anisotropy, the frequency spectrum of strongly growing modes becomes narrower and the real frequency at maximum growth rate asymptotically approaches $\omega=0.8\Omega_i$.

Figures 4 and 5 are plots of the real frequency and the growth rate versus normalized shear for ion temperature anisotropies of 1, 2, 4, and 6. Each curve was generated by keeping all quantities except parallel flow shear constant and maximizing the growth rate over the propagation angle. Figures 4 and 5 illustrate the effects of ion thermal anisotropy at different values of normalized shear. In addition to the frequency upshift that accompanies an increase in thermal anisotropy, Fig. 4 shows how the magnitude of the frequency shift changes with normalized parallel flow shear. As the shear is increased, the shift in real frequency becomes less dramatic (although still significant). Thus, the real frequency

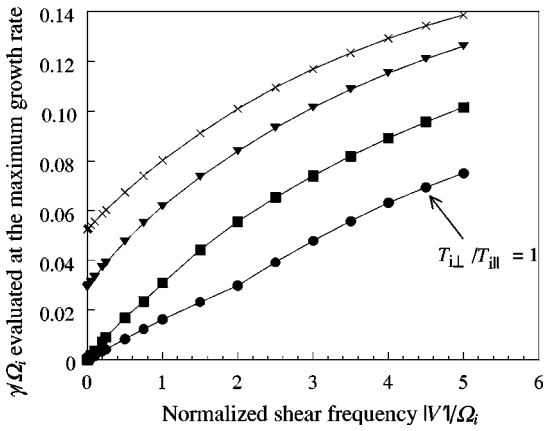

FIG. 5. Growth rate versus normalized shear for (●) $T_{i\perp}/T_{i\|}=1$, (■) $T_{i\perp}/T_{i\|}=2$, (▼) $T_{i\perp}/T_{i\|}=4$, and (×) $T_{i\perp}/T_{i\|}=6$. For these calculations, $T_{i\perp}/T_{e\perp}=0.3$, $M_i/M_e=29\,392$, and $V_d/v_{i\text{th}\perp}=60$.

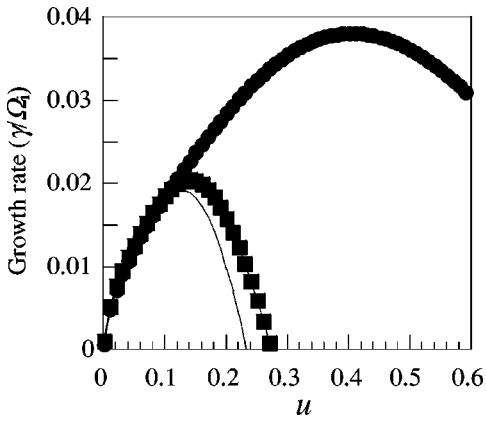

FIG. 6. Approximate growth rate versus propagation angle for (solid line) $T_{i\perp}/T_{i\|}=1$ and $T_{i\perp}/T_{e\perp}=0.3$, (●) $T_{i\perp}/T_{i\|}=2$ and $T_{i\perp}/T_{e\perp}=0.3$, (■) $T_{i\perp}/T_{i\|}=2$ and $T_{i\perp}/T_{e\perp}=0.6$. For these calculations $M_i/M_e=29\,392$, $V_d/v_{i\text{th}\perp}=60$, and $|V_d'|/\Omega=0.5$.

upshifts with increasing anisotropy or increasing shear. A shift due to an increase in either parameter tends to saturate at a real frequency slightly below the ion cyclotron frequency for the parameters used here.

Figure 5 shows that the growth rate of an ion acoustic plasma wave increases both with $T_{i\perp}/T_{i\|}$ and with normalized shear. In the isotropic case, the growth rate becomes extremely small in the absence of shear, thereby confirming that a perpendicular gradient in the parallel flow is responsible for this instability. However, the anisotropic cases still have a substantial growth rate at small values of normalized shear. This suggests that the equilibrium flow (i.e., current) and temperature anisotropy are sufficient to excite low frequency, ion-acoustic modes in such thermally anisotropic plasmas. The growth rate also increases significantly with the shear parameter, σ. A maximum in growth rate was not observed for the range of plasma parameters investigated.

Assuming the growth rate is small compared to the real frequency, analytic expansion of the dispersion relationship around the approximate solution yields an expression for the growth rate. In terms of the dimensionless parameters defined in Appendix A, the approximate growth rate is

$$\gamma = -u\sigma\sqrt{\pi b/8\tau^3\hat{T}_e}\,\sigma^3\sqrt{\hat{T}_i^3/\tau\hat{T}_e}\,e^{-\sigma^2\hat{T}_i/2\tau\hat{T}_e} + \sqrt{\tau^3\hat{T}_e^3/\mu}\,(\sigma/\sqrt{\tau\hat{T}_e}-\hat{V}_d). \tag{9}$$

Equation (9) as a function of u is shown in Fig. 6 for two different values of ion temperature anisotropy and two different values of the ion to electron temperature ratio, τ. Note that for $T_{i\perp}/T_{i\|}=1$ and $T_{i\perp}/T_{i\|}=2$ (with $\tau=0.3$) the approximate growth rate peaks at values of u consistent with the numerical growth rate calculations shown in Fig. 2. The magnitudes of the peaks are also consistent with the numerical growth rate calculations shown in Fig. 5. For larger anisotropies, higher harmonic terms must be included and the simplified expression of Eq. (9) differs significantly from the complete numerical calculations. Numerical evaluation of Eq. (9), as shown in Fig. 6, confirms that, to first order, the maximum growth rate of the instability occurs at increasing values of u as the ion temperature anisotropy increases.

IV. DISCUSSION

The dispersion relation derived here is a generalization of previous work by Ganguli *et al.*[12] to include thermal anisotropy and parallel flow shear. Although the dispersion relation is valid for any value of temperature anisotropy, both the analytic expression and the numerical results are only valid in the weak shear, $\rho_i \ll L = V_d/(dV_d/dx)$, limit. The perturbed distribution functions described in this work also represent a generalization of the work of Skiff *et al.*[27] to include velocity shear. Since the perturbed distribution function is a measurable plasma quantity, the profound effect of shear in the parallel flow is of significant experimental interest. Inclusion of sheared parallel flow introduces dependence on both k_y and k_z into the expression for $f_1(v_\|)$.[31]

The numerical solutions to the dispersion relation demonstrate that ion thermal anisotropy can play an important role in changing the frequency, growth rate, and propagation angle of ion acoustic instabilities in the presence of a perpendicular gradient in the field-aligned flow. According to Figs. 2 and 4, the real frequency corresponding to the largest growth rate upshifts significantly for ion-acoustic waves as $T_{i\perp}/T_{i\|}$ increases. The upshift saturates at a real frequency of approximately $\omega_r=0.8\Omega_i$, an increase of almost 700%. The frequency upshift in an ion acoustic wave is actually a two-step process. As the anisotropy is increased, the value of u corresponding to the maximum growth rate also increases (Fig. 3). Since $k_y\rho_i$ is held constant as $u=k_\|/k_y$ is varied, a higher value of u is equivalent to a higher value of $k_\|/\rho_i$. Given the approximate relationship between the real frequency and $k_\|$, Eqs. (7), it is not surprising that the real frequency shifts up as $k_\|$ increases.

An interesting characteristic of the upshift is that it tends to saturate at high values of shear. Thus, increasing anisotropy at high shear has a much less dramatic effect on the real frequency. For example, increasing the value of $T_{i\perp}/T_{i\|}$ from unity to six results in a frequency upshift of approximately 800% for the lowest normalized shear value shown in Fig. 4, while the frequency upshifts only 10% for the highest shear value shown in Fig. 4. However, the growth rate shows only

a slight saturation at the highest anisotropy (Fig. 5) and the increase in growth rate due to increased anisotropy appears unaffected by the magnitude of the shear.

A critically important facet of these calculations is the interpretation of an increasing ion temperature anisotropy. In other words, is the perpendicular ion temperature increasing relative to the parallel temperature (interpretation #1), or is the parallel ion temperature decreasing relative to the perpendicular (interpretation #2)? The ambiguity exists because, apart from the normalized gyroradius and relative drift velocity terms that are held constant, only the ion temperature anisotropy appears in the dimensionless form of the dispersion relation (see Appendix A). Under interpretation #2, holding the normalized gyroradius (b) and the ion to electron perpendicular temperature ratio (τ) constant while varying the ion temperature anisotropy permits consistent comparison of different anisotropy cases, i.e., the ion temperature anisotropy can be varied without also changing other plasma parameters. The physical constraints of interpretation #2 suggest that the increased growth rate of the ion acoustic instability at large anisotropies is due to the reduced ion Landau damping that would be expected in a plasma with a lower parallel ion temperature. The increases in real frequency and parallel wave number, u, of the ion acoustic instability with decreasing parallel ion temperature and fixed electron temperature are consistent with Fig. 1(b) of Ref. 31 if the relevant plasma parameter is the ratio $T_{e\|}/T_{i\|}$. Although Kindel and Kennel found that real frequency of the ion acoustic instability approached $1.5\Omega_i$ for $T_e/T_i \gg 1$, not $0.8\Omega_i$ as found in this work, their calculations were for an isotropic plasma without parallel velocity shear.[31] For isotropic plasmas without shear, Eq. (4) reduces to the same expression used by Kindel and Kennel.[31] For anisotropic plasmas without shear, the numerical solutions to Eq. (4) are also consistent with previous calculations in the limit $k_y\rho > 1$.[33]

Under interpretation #1, an increased ion temperature anisotropy implies an increased perpendicular ion temperature, decreased relative drift velocity, and increased perpendicular and parallel ion electron temperatures (the electron temperature components change because τ and $\hat{T}_e$ were held fixed during the analysis). According to the approximate dispersion relation, the real frequency of the ion acoustic instability increases with increasing electron temperature. Thus, it could be argued that the observed dependence of the real frequency of the ion acoustic instability on ion temperature anisotropy is due to increased parallel electron temperature. However, increased parallel electron temperatures cannot explain the increased growth rates [Eq. (9) is independent of absolute electron temperature] or the saturation in the upshift of the real frequency. For a given parallel wave number, the real frequency should increase as the square root of the ion temperature anisotropy (via the changing parallel electron temperature). Instead, the real frequency of the ion acoustic instability increases much more rapidly than the square root of the ion temperature anisotropy (see Fig. 2) and then saturates. A more likely explanation is that the critical parameter, as with interpretation #2, is the ratio $T_{e\|}/T_{i\|}$. Under interpretation #1, $T_{i\|}$ is fixed while $T_{e\|}$ increases. Kindel and Kennel's isotropic, shearless calculations showed a similar saturation in the real frequency of the ion acoustic instability at large values of T_e/T_i.[31]

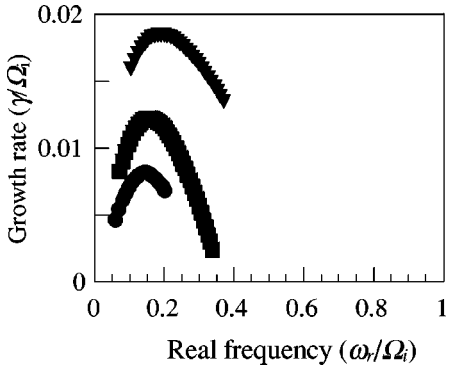

FIG. 7. Growth rate versus real frequency maximized over u and b for plasmas with (●) $T_{i\perp}/T_{i\|}=1$ and $\tau=0.3$, (■) $T_{i\perp}/T_{i\|}=2$ and $\tau=0.6$, and (▼) $T_{i\perp}/T_{i\|}=4$ and $\tau=1.2$. For these calculations, $M_i/M_e=29\,392$, $V_d/v_{i\mathrm{th}\perp}=60$, and $|V_d'|/\Omega=0.5$.

To further explore interpretation #1, the effect of increased ion temperature anisotropy in a plasma for which the electron temperature components and the parallel ion temperature were held constant was investigated. The electron temperature components were held constant by adjusting the ratio of perpendicular ion to electron temperature for each value of ion temperature anisotropy studied. For example, if the ion temperature anisotropy was increased, τ was increased by the same factor. Note that for completeness, the relative drift velocity should also be similarly increased. However, because only a weak dependence of the frequency for peak ion acoustic instability growth rate on relative drift was observed, the relative drift was held constant. The growth rate of the ion acoustic mode versus real frequency maximized over b and u for three different ion temperature anisotropies and appropriately adjusted values of τ is shown in Fig. 7. As the ion temperature anisotropy increases, there is a small increase in the growth rate and a small upshift in the real frequency of the strongest growing mode. As can be seen in the $\tau=0.6$ curve in Fig. 6, the shift in the propagation angle for the strongest growing mode as a function of ion temperature anisotropy is also much smaller when the ion to electron temperature ratio is adjusted to keep the electron temperature constant. These results confirm that changes in the ratio $T_{e\|}/T_{i\|}$ (held fixed in Fig. 7) are responsible for the dramatic upshift in real frequency seen in Fig. 2 and that both interpretations of varying the ion temperature anisotropy are identical when the effect on $T_{e\|}/T_{i\|}$ is considered. The physics of the ion temperature anisotropy dependence seen in these calculations is fundamentally a reflection of the effects of differing ion and electron parallel temperatures.

Laboratory experiments in which the ratio $T_{e\|}/T_{i\|}$ and the parallel flow shear can be controlled should be able to confirm the theoretical predictions presented in this work. Although driven by a different physical mechanism, instabilities due by shear in the transverse flow have shown a surprising resilience to increased plasma collisionality.[34] Since parallel shear modified ion acoustic instabilities have

already been observed experimentally, it is likely that the effects of temperature anisotropy on mode frequency and growth rate will be observable even in moderately collisional plasmas. Strong parallel flows associated with wave activity near the ion cyclotron frequency have been observed in our thermally anisotropic, collisional, laboratory plasmas.[25] If those parallel flows are also inhomogeneous, the shear modified, thermally anisotropic ion acoustic instability could be responsible for the observed low-frequency waves. Experiments designed to measure the shear in the parallel flow in our plasmas are in progress at this time. Inclusion of collisional effects in the theory is planned for future work.

ACKNOWLEDGMENTS

We thank Dr. Valeriy Gavrishachaka for providing a copy of the original FORTRAN code and helpful discussions, Professor Fred Skiff for helpful discussions concerning perturbed distribution function calculations, and Professor Mark Koepke for helpful comments. One of us (R.S.S.) thanks NRL for their hospitality during his stay at NRL.

This work was performed with support from National Science Foundation Grant No. ATM-99988450, the Office of Naval Research, the Naval Research Laboratory (NRL), NASA, and the West Virginia University Graduate Student Travel Grant program.

APPENDIX A: DIMENSIONLESS DISPERSION RELATIONS

The dispersion relation can be expressed as

$$Q(\hat{b},\hat{\omega},\hat{T}_i,\hat{T}_e,\tau,\hat{V}_d',\hat{V}_d,u,\mu)=0, \tag{A1}$$

where

$$Q=O(k^2\lambda_{Di\perp}^2)+\hat{T}_i + \sum_{n=-\infty}^{\infty}\Gamma_n(b)F_{ni}+\tau\hat{T}_e(1-F_{0e}),$$

where

$$F_{ni}=\hat{T}_i^{1/2}\left[\frac{n(1-\hat{T}_i)+\hat{\omega}\hat{T}_i}{u\sqrt{2\hat{b}}}\right]Z\left(\frac{(\hat{\omega}-n)\hat{T}_i^{1/2}}{u\sqrt{2\hat{b}}}\right) - \frac{\hat{T}_i\hat{V}_d'}{u}\left[1+\left(\frac{(\hat{\omega}-n)}{u\sqrt{2\hat{b}}}\hat{T}_i^{1/2}\right)Z\left(\frac{(\hat{\omega}-n)}{u\sqrt{2\hat{b}}}\hat{T}_i^{1/2}\right)\right],$$

$$F_{0e}=\left(\frac{\tau^{1/2}\hat{T}_e^{1/2}}{\sqrt{2}\mu^{1/2}}\left(\frac{\hat{\omega}}{u\sqrt{\hat{b}}}-\hat{V}_d\right)\right)Z\left(\frac{\tau^{1/2}\hat{T}_e^{1/2}}{\sqrt{2}\mu^{1/2}}\left(\frac{\hat{\omega}}{u\sqrt{\hat{b}}}-\hat{V}_d\right)\right) + \frac{\hat{V}_d'}{u\mu}\left[1+\left(\frac{\tau^{1/2}\hat{T}_e^{1/2}}{\sqrt{2}\mu^{1/2}}\left(\frac{\hat{\omega}}{u\sqrt{\hat{b}}}-\hat{V}_d\right)\right)\times Z\left(\frac{\tau^{1/2}\hat{T}_e^{1/2}}{\sqrt{2}\mu^{1/2}}\left(\frac{\hat{\omega}}{u\sqrt{\hat{b}}}-\hat{V}_d\right)\right)\right],$$

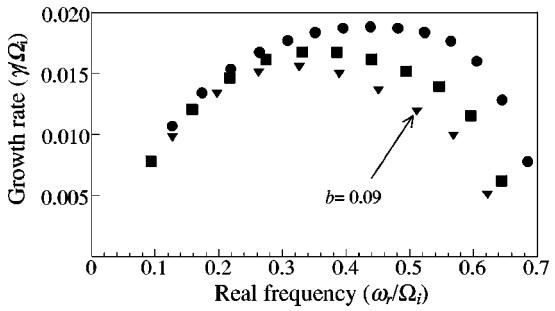

FIG. 8. Growth rate versus real frequency for (●) $b=0.04$, (■) $b=0.0675$, and (▼) $b=0.09$. For these calculations, $T_{i\perp}/T_{i\|}=2$, $T_{i\perp}/T_{e\perp}=0.3$, $M_i/M_e=29\,392$, $V_d/v_{i\mathrm{th}\perp}=60$, and $|V_d'|/\Omega=0.5$.

$\Gamma(b)\equiv I_n(b)e^{-b}$, $\hat{b}\equiv(k_y\rho_i)^2$, $\hat{\omega}\equiv\omega/\Omega$, $\hat{T}_i\equiv T_{i\perp}/T_{i\|}$, $\hat{T}_e\equiv T_{e\perp}/T_{e\|}$, $\tau\equiv T_{i\perp}/T_{e\perp}$, $\hat{V}_d'\equiv V_d'/\Omega$, $\hat{V}_d=V_d/v_{i\mathrm{th}\perp}$, $u\equiv k_\|/k_y$, and $\mu\equiv M_i/M_e$. The zero-order expression for the real frequency, Eq. (7), in terms of these dimensionless variables is

$$\hat{\omega}\approx u\sigma\sqrt{\frac{b}{\tau\hat{T}_e}}. \tag{A2}$$

APPENDIX B: MAXIMIZATION OVER NORMALIZED GYRORADIUS

The maximum growth rates used in Figs. 2–5 for the ion acoustic mode were obtained by fixing the normalized gyroradius, b, and varying propagation angle of the instability, u. However, for a complete investigation, the peak growth rate as a function of both quantities must be determined. Fortunately, the amplitude of peak growth rate and the real frequency at which the peak growth rate occurs are relatively insensitive to b. Figure 8 shows the growth rate versus real frequency for different values of b in a $T_{i\perp}/T_{i\|}=2$ plasma. Figure 9 shows the growth rate versus real frequency for different values of b in a $T_{i\perp}/T_{i\|}=5$ plasma. Each graph was obtained by maximizing over u (as done in the previous figures) for a fixed value of b.

Figure 8 demonstrates that maximizing over b yields an additional modest upshift in the real frequency at which the maximum growth rate occurs. Thus, the upshift of the ion acoustic instability with thermal anisotropy seen in Fig. 2

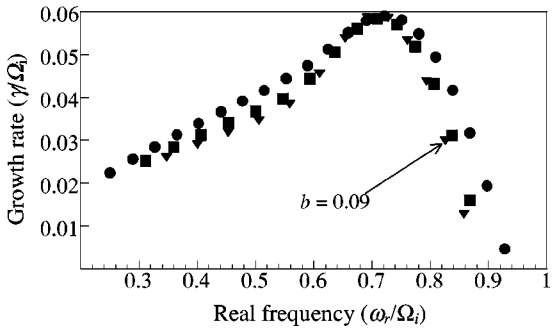

FIG. 9. Growth rate versus real frequency for (●) $b=0.04$, (■) $b=0.0675$, and (▼) $b=0.09$. For these calculations, $T_{i\perp}/T_{i\|}=5$, $T_{i\perp}/T_{e\perp}=0.3$, $M_i/M_e=29\,392$, $V_d/v_{i\mathrm{th}\perp}=60$, and $|V_d'|/\Omega=0.5$.

would increase if b the growth rate were also maximized over the normalized gyrofrequency. Figure 9 demonstrates that the effect of maximizing over b decreases with increasing $T_{i\perp}/T_{i\parallel}$. Since maximizing over b increases the frequency shift at lower values of $T_{i\perp}/T_{i\parallel}$ and has almost no effect at higher values of $T_{i\perp}/T_{i\parallel}$, maximizing only over u shows the essence of the thermal anisotropy effects on the real frequency and the growth rate of the ion acoustic mode.

[1] N. Ivchenko, G. Marklund, K. Lynch, D. Pietrowski, R. Torbert, F. Primdahl, and A. Ranta, Geophys. Res. Lett. **6**, 3365 (1999).
[2] G. Marklund, L. Blomberg, C. Falthammar, and P. Lindqvist, Geophys. Res. Lett. **21**, 1859 (1994).
[3] E. V. Mishin and M. Forster, Geophys. Res. Lett. **22**, 1745 (1995).
[4] R. E. Ergun, C. W. Carlson, J. P. McFadden, F. S. Mozer, G. T. Delory, W. Peria, C. C. Chaston, M. Temerin, R. Elphic, R. Strangeway, R. Pfaff, C. A. Cattell, D. Klumpar, E. Shelly, W. Peterson, E. Moebius, and L. Kistler, Geophys. Res. Lett. **25**, 2025 (1998).
[5] M. André, G. B. Crew, W. K. Peterson, A. M. Persoon, C. J. Pollock, and M. J. Engebretson, J. Geophys. Res. **95**, 20809 (1990).
[6] M. André, P. Norqvist, L. Andersson, L. Eliasson, A. Eriksson, L. Blomberg, R. Erlandson, and J. Waldemark, J. Geophys. Res. **103**, 4199 (1998).
[7] K. A. Lynch, R. L. Arnoldy, P. M. Kintner, and J. Bonnell, Geophys. Res. Lett. **23**, 3293 (1996).
[8] P. Norqvist, M. André, and M. Tyrland, J. Geophys. Res. **103**, 23459 (1998).
[9] D. J. Knudsen, J. H. Clemmons, and J.-E. Wahlund, J. Geophys. Res. **103**, 4171 (1998).
[10] M. E. Koepke, J. J. Carroll III, and M. W. Zintl, Phys. Plasmas **5**, 1671 (1998).
[11] G. Ganguli, Phys. Plasmas **5**, 1544 (1997).
[12] G. Ganguli, M. J. Keskinen, H. Romero, R. Heelis, T. Moore, and C. Pollock, J. Geophys. Res. **99**, 8873 (1994); G. Ganguli, Y. C. Lee, and P. J. Palmadesso, Phys. Fluids **31**, 823 (1988).
[13] V. V. Gavrishchaka, Gurudas I. Ganguli, and Supriya B. Ganguli, Phys. Rev. Lett. **80**, 728 (1998).
[14] V. V. Gavrishchaka, Supriya B. Ganguli, and Gurudas I. Ganguli, J. Geophys. Res. **104**, 12 683 (1999).
[15] N. D'Angelo, Phys. Fluids **8**, 1748 (1965).
[16] J.-E. Wahlund, P. Louran, T. Chust, H. de Feraudy, R. Roux, B. Holback, P.-O. Dovner, and G. Holmgren, Geophys. Res. Lett. **21**, 1831 (1994).
[17] J.-E. Wahlund, P. Louran, T. Chust, H. de Feraudy, R. Roux, B. Holback, B. Cabrit, A. I. Ericksson, P. M. Kintner, M. C. Kelley, J. Bonnell, and C. Chesney, Geophys. Res. Lett. **21**, 1835 (1994).
[18] J.-E. Wahlund, A. I. Eriksson, B. Holback, M. H. Boehm, J. Bonnell, P. M. Kintner, C. E. Seyler, J. H. Clemmons, L. Eliasson, D. J. Knudsen, P. Norqvist, and L. J. Zanetti, J. Geophys. Res. **103**, 4343 (1998).
[19] E. Agrimson, N. D'Angelo, and R. L. Merlino, Phys. Rev. Lett. **86**, 5282 (2001).
[20] C. Teodorescu, E. W. Reynolds, and M. E. Koepke, Phys. Rev. Lett. **88**, 185003 (2002).
[21] V. V. Gavrishchaka, G. Ganguli, W. A. Scales, S. P. Slinker, C. C. Chaston, J. P. McFadden, R. E. Ergun, and C. W. Carlson, Phys. Rev. Lett. **85**, 4285 (2000).
[22] T. H. Stix, *The Theory of Plasma Waves* (American Institute of Physics, New York, 1962), pp. 247–262.
[23] R. C. Davidson and Joan M. Ogden, Phys. Fluids **18**, 1045 (1975).
[24] B. J. Anderson, S. A. Fuselier, S. P. Gary, and R. E. Denton, J. Geophys. Res. **99**, 5877 (1994).
[25] E. E. Scime, Paul A. Keiter, Matthew M. Balkey, Robert F. Boivin, John L. Kline, Melanie Blackburn, and S. Peter Gary, Phys. Plasmas **7**, 2157 (2000).
[26] R. S. Spangler, Jr., M.S. thesis, West Virginia University (2001).
[27] F. Skiff and F. Anderegg, Phys. Rev. Lett. **59**, 896 (1987).
[28] M. Sarfaty, S. DeSouza Machado, and F. Skiff, Phys. Plasmas **3**, 4316 (1996).
[29] J. L. Kline, E. E. Scime, P. A. Keiter, M. M. Balkey, and R. F. Boivin, Phys. Plasmas **6**, 4767 (1999).
[30] R. A. Stern and J. A. Johnson, Phys. Rev. Lett. **34**, 1548 (1975).
[31] S. DeSouza-Machado, Ph.D. dissertation, University of Maryland (1996).
[32] J. M. Kindel and C. F. Kennel, J. Geophys. Res. **76**, 3055 (1971).
[33] Kai Fong Lee, J. Plasma Phys. **8**, 379 (1972).
[34] M. E. Koepke, M. W. Zintl, and T. N. Good, Geophys. Res. Lett. **25**, 3095 (1998).